Pergamon

Int. J. Impact Engng, Vol. 17, pp. 121–130, 1995

0734-743X/95 $9.50+0.00

BUILDING CHARACTERISTICS INTO A SHAPED CHARGE TO ACHIEVE UNIQUE PERFORMANCE REQUIREMENTS

Ronald E. Brown, Mark E. Majerus, J. Scott Lewis

Titan Research & Technology Division, Titan Corporation, 5117 Johnson Drive, Pleasanton, Ca 94588

Summary–Traditionally, shaped charges have been designed and used to penetrate long line-of-sight targets. This paper presents the results of three successful design efforts in which the performance goals were quite different: the defeat of reactive appliqués, the localized consolidation of jet mass, and the demonstration of ductile, tungsten jetting. Each design has required that particular attention is devoted to the nature of the liner collapse and the subsequent jetting. Finite difference hydrocodes have provided the level of detail necessary to observe the critical phenomenon. The approaches taken, the computational techniques used and comparisons between experimental results, prediction and performance goals are discussed.

INTRODUCTION

Traditionally, shaped charges have been designed and used to penetrate through long line-of-sight monolithic and spaced target arrays composed of ceramic and metallic components. In order to defeat the more difficult targets, greater jet length is required. This need is usually addressed by increasing the jet tip velocity and jet breakup time. These characteristics challenge the limitations of coherent flow and tensile failure of the liner material. In the last twenty years there has also been much interest in dense and fast-sound-propagating liner materials for purposes of achieving greater penetration depths. This is reflected by the interests in tantalum, uranium, tungsten, and molybdenum.

There are a number of problems, however, that require entirely different approaches to shaped charge design. For example, some targets are more lethaly defeated by punching a large hole rather than a deep hole, or where the jet is required to not only penetrate, but also activate a target in a preferred manner, e.g. reactive armor. Other interesting problems involve affecting desirable material properties during liner collapse, e.g. brittle-to-ductile transitions, to increase jet penetration performance.

The increasing accuracies of material response models and multi-dimensional, multi-material finite difference codes, provide capabilities for more detailed investigation of shaped charge jetting and better means for designing characteristics in a charge for applications other than (but including) deep penetration. We discuss in this paper three examples in which these improved capabilities have helped to successfully develop constant jet segment(s) and which have played an important part in improving the effectiveness of tungsten as a shaped charge liner material.

DESIGN TOOLS AND APPROACH

A version of the CTH finite difference, Eulerian hydrocode developed by Sandia National Laboratories[1] was employed for this work. An Eulerian code offers a facile method of estimating severe material deformation and partitioning during liner collapse and jet formation, and avoids the need for rezoning and cumulative errors that might result. The improved interfacial boundary logic in the code is a vast improvement over that in Sandia-CSQ, from which we reported mechanistic details of the partitioning process[2]. Lagrangian tracer particles that move with the material are used to monitor pressure, temperature and motion.

Special routines, for interrogating the material flow and mass in the jet, are integrated into the code.

We also employ techniques for predicting flow through the stagnation region so as not to exceed the coherency limit, based on classical treatments by Walsh[3], and Chou and Carleone[4]. It is commonly agreed that the flow velocity, V_f, (see Figure 1) at the stagnation surface of collision has to be lower than some limiting value c^* related to the sound velocity in the liner. This stagnation surface is the moving reference plane at which the liner material either flows into the jet or into the slug. Harrison proposed a threshold for coherent copper jetting of 1.23 times ambient sound velocity[5]. Chanteret[6] and Walker[7] generally agree and have proposed constant values for other materials, however the latter disagrees that incoherence is due to the formation of an attached shock at the collision surface and argues that the relevant sound speed is the low pressure longitudinal sound speed for elastic-plastic solids. Brown et. al.[8], concluded that pressure should be taken into account and that the 1.23*c factor for copper just happens to coincide with the sound velocity at compressions typically experienced during the explosively driven collapse of a conic liner. Consistent with this approach, we estimate the stagnation velocity, V_S, for any local condition by tracking the progress of the peak pressure surface constituting the stagnation surface or point. The jet velocity is simply the sum of the flow velocity, V_f, of the material into the stagnation region and the stagnation region velocity, V_S. By subtracting the resultant jet velocities from the stagnation velocity, V_S, the flow velocities can be estimated. We then compare these flow velocities with reported sound velocities at pressure[9].

COMPACTING JETTING CHARGE

The first example involves a charge design derived for penetrating an armor target protected by a spaced metal-explosive sandwich (e.g., see Mayseless et. al. [10]). For purposes of negating the effects of the explosive sandwich, we derived a charge that could generate a jet stream composed of a constant velocity bow segment of sufficient density, length and velocity, to punch holes large enough through the metal components of the sandwich for the residual jet to escape through before the plates could move to disturb the jet. The variable-angle, variable-thickness, aluminum-lined, 100 mm diameter, LX-14 - filled, ring-initiated charge, shown in Figure 2, was designed to meet the performance objective. It was designed to generate a 12 km/sec constant-velocity segment at the lead end of a stretchy jet terminating at 4 km/sec. The predicted jet velocity profile is shown in Figure 3.

Aluminum was chosen because of its high sound velocity and low density. Molybdenum would have been as satisfactory a liner material based on its intrinsic sound propagating property. However, in order to punch the size holes required to meet the basic strategy, we needed a low density material because the rate of energy expended per penetration length is inversely dependent on jet density.

During the initial design iterations we found that the liner compressions reached from point initiation were insufficient to sustain coherent flow, unless we were to abandon our basic design approach. The larger angle impact from peripheral initiation satisfied our requirement, allowing a design that could meet the basic jetting objectives well within the stability limit.

Figure 4 shows a radiograph of the constant-velocity rod generated at the leading edge of the jet stream by this charge. The velocity of this 12 cm long leading particle is 12.3 km/sec. The maximum flow velocity contributing to the resultant jet velocity is estimated to be 6.1 km/sec., which is well within the stability limit at the pressures exerted on the material in the stagnation region. This is an example of the importance of waveshaping. The directionality as well as the forces exerted on the liner, in this case, generate the pressure levels to support coherent flow and the resultant 12.3 km/sec jet velocity[11]. Conversely, there are examples of aluminum jets that bifurcate at lower velocities[12,13].

Figure 5 shows a radiograph of the residual jet after penetrating the explosive sandwich and a spaced steel plate. The target is 60° from the flight line of jet. Figure 6 shows a jet from the same charge after normal impact and penetration through an equivalent thickness of steel. From comparisons of jet appearance and position relative to a third plate encounter, we conclude that the hole opening made by the jet was large enough to avoid intersecting (a) back surface spall, resulting from oblique impact, and (b) the explosively accelerated plates that were eventually set in motion by the jet impact.

The concentrated energy in this jet is further demonstrated (see Figure 7) by the perforation

it makes against reinforced concrete (compressive yield strength 4000 psi). The minimum diameter of the hole through this 200 mm thick target is 220 mm.

CHARGE FOR PRODUCING DISCRETE HIGH ENERGY JET SEGMENTS

The second case exemplifies a problem that dictated a design solution for generating two discrete and nearly equal energy segments within the body of the jet, in addition to the jet tip. There are a number of applications for such a charge. Aseltine[14], for example, developed oil well perforating charges that produce a jet with a "moving" bulge, for punching large holes through well casings at close standoffs. He accomplished this by incorporating, by design, a reverse velocity gradient in the middle of the jet. In order to allow manufacturing control of the gradient, Aseltine used shaped tooling to vary the density of the explosive. He apparently also achieved similar results by incorporating thickness discontinuities in the confinement body.

In the case reported herein, two fixed and nearly equal energy segments are incorporated within a jet stream by liner design. Zero velocity gradients are incorporated at designated axial positions within the velocity profile, as illustrated in Figure 8. We are careful in the design to avoid excessive bulging that could cause jet curvature, because the charge must maintain effectiveness over long standoffs. We also avoid a large positive velocity gradient from the liner apex so that there is enough remaining mass to distribute into the velocity plateaus.

A jet from a charge designed to include these characteristics is shown in Figure 9. In this doubly exposed radiograph, there is shown an image of the liner prior to detonation impact and the resultant slug and jet after liner collapse.

SHEAR RATE CONTROL FOR TUNGSTEN DUCTILITY

We show in a final example, the possible importance of shear on tungsten jet ductility. During an on-going development project, we found that large radial velocity gradients across the jet radius can cause radical departures in jet appearance and an increased rate of breakup. The particles formed are more brittle-like in appearance. Increased jet mass might also contribute to this observation.

Figures 10 and 11 show radiographs of two tungsten jets from two different designs. Figure 10 shows a tip-to-tail composite of Design #1, and Figure 11 compares corresponding mid-length sections of Designs #1 and #2. Design #1 exhibits good ductility with characteristic necking. Design #2 contains more mass below 7 km/sec and, based on CTH computations, contains much larger radial velocity gradients (see Figure 12). From comparative analyses of five designs (including Designs #1 and #2) which generated jets with similar mass-velocity distributions, but increasing mass below 7 km/sec, we found decreasing ductility. As mass increases, the radial velocity gradients increase. We believe that these observations are consistent with Hirsh's[15] postulates regarding the effect that internal flow has on jet elongation and stability. In going from Design #1 to Design #2, the increase in jet mass has perhaps created a situation where jet shrinkage is caused more by tension along the axis of symmetry than by internally directed radial tension.

CONCLUSIONS

In each of these three design studies, unique jet characteristics are required for improved lethality against the intended targets. This differs from the usual requirement of longer jets required for deeper penetration. The level of understanding of critical liner collapse components is instrumental in being able to control the evolution of a shaped charge design. The improved computational tools now provide the level of detail that is required to note the differences needed in order to optimize a design for specialty applications and to reach new performance levels.

REFERENCES

1. J. M. McGlaun, E. S. Hertel, S. L. Thompson, L. N. Kmetyk, M. G. Elrick, *CTH User's Manual*, Sandia National Laboratories, (1991).
2. R. E. Brown and A. Nordell, Kinematics of shaped charge liner collapse and jet formation, *11th Intl. Symposium on Ballistics*, Vol. **2**, (WM-3/1) p. 25, Brussles, Belgium (1989).

3. J. M. Walsh, R. G. Shreffler and F. J. Willig, Limiting conditions for jet formation in high velocity collisions, *J. Appl. Physics*, **24**, p. 349, (1953).
4. P. Chou, Carleone and R. R. Karpp, Criteria for jet formation from impinging shells and plates, *J. Appl. Physics* **47**, 2975, (1976).
5. J. T. Harrison, BASC, An analytical code for calculation of shaped charge properties, *6th Int'l. Symposium on Ballistics*, P. 253, Orlando, Fl (1981).
6. P. Y. Chanteret, Studies of maximum velocities for coherent shaped charge jets, *13th.Int'l.Symposium on Ballistics*, Vol. **2**, (WM-3/1) p. 327, Stockholm, Sweden (1992).
7. J. Walker, Incoherence of shaped charge jets, *14th Int'l. Symposium on Ballistics*, Vol, **2**, (WM18) p. 165, Quebec, Canada (1993).
8. R. E. Brown, M. E. Majerus, R. F. Johnson, H. A. Hope and J. A. Kotyk, Dynamic model for predicting shaped charge stability, 12th Int'l. Symposium on Ballistics, Vol. **1**, p. 317, San Antonio, TX (1990).
9. S. P. Marsh, LASL shock hugoniot data, *University of Caifornia Press*, Berkeley, Ca (1980).
10. M. Mayseless, E. Marmo, N. Gov, Y. Kivity, J. Falcovitz and D. Tzur, Interaction of a shaped charge jet with reactive or passive cassettes, *14th Int'l. Symposium on Ballistics*, Vol. **2**, (TB24) p. 439, Quebec, Canada (1993).
11. Similar effects are accomplished using a subcaliber liner, for example see: J. Bol H. Baumgardt and V. Friehmelt, Shaped charge technique of producing ultrafast, heavy, single projectiles for hypervelocity impact tests on space debris protection shields, *14th Int'l. Symposium on Ballistics*, Vol. **2**, (WM19) p. 173, Quebec, Canada (1993).
12. See for example, P. Y. Chanteret, Studies of maximum velocities for coherent shaped charge jets, *13th Int'l. Symposium on Ballistics*, Vol. **2**, (WM-3/1) p. 327, Stockholm, Sweden (1992).
13. K. G. Cowan, R. J. Kelly, J. P. Curtis, P. A. F. Callow, and B. Bourne, On the prediction of incoherent shaped charge jets, *14th Int'l. Symposium on Ballistics*, Vol. **2**, (WM4) p. 39, Quebec, Canada (1993).
14. C. Aseltine, Design of a charge with a double inverse velocity gradient, *13th Int'l. Symposium on Ballistics*, Vol. **2**, (WM-25/1) p. 505, Stockholm, Sweden (1992).
15. E. Hirsch, How does the shaped charge jet become hollow?, *14th Int'l. Symposium on Ballistics*, Vol. **2**, (WM3) p. 29, Quebec, Canada (1993).

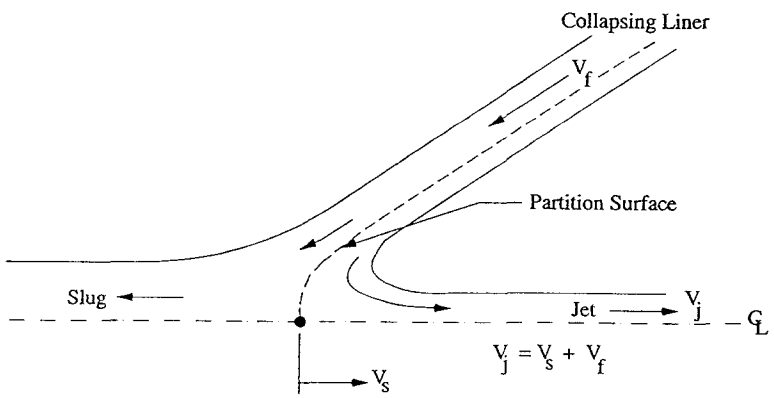

Figure 1. Flow Diagram of Liner Material Through Stagnation Region (Moving Coordinate System.)

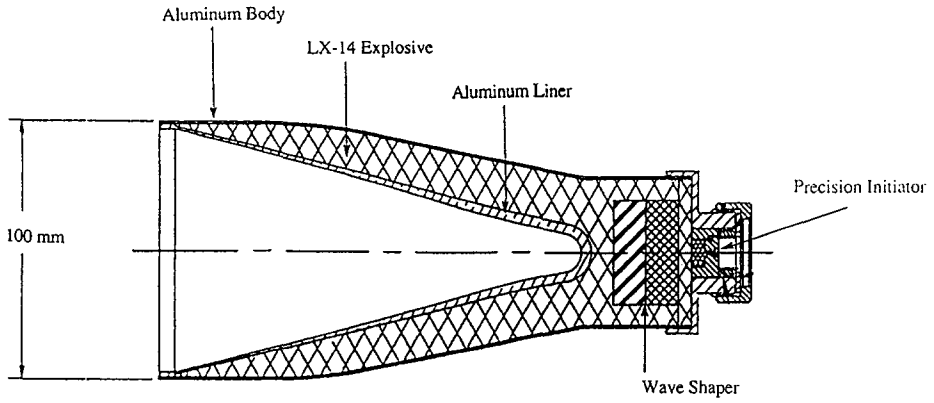

Figure 2. Description of the 100 mm Charge Aluminum Lined Charge Designed to Generate a Stable Constant Velocity 12.3 km/sec Rod.

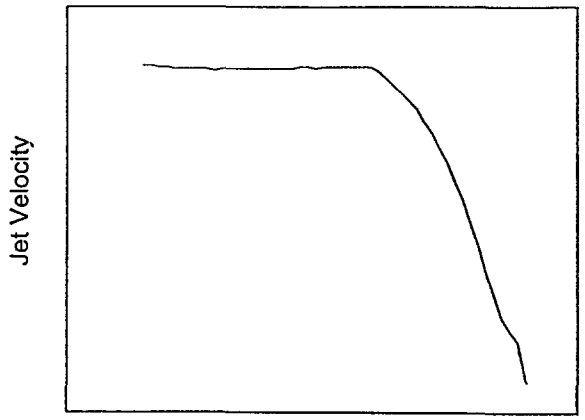

Figure 3. Jet Velocity and Jet Mass Profile Calculated with CTH.

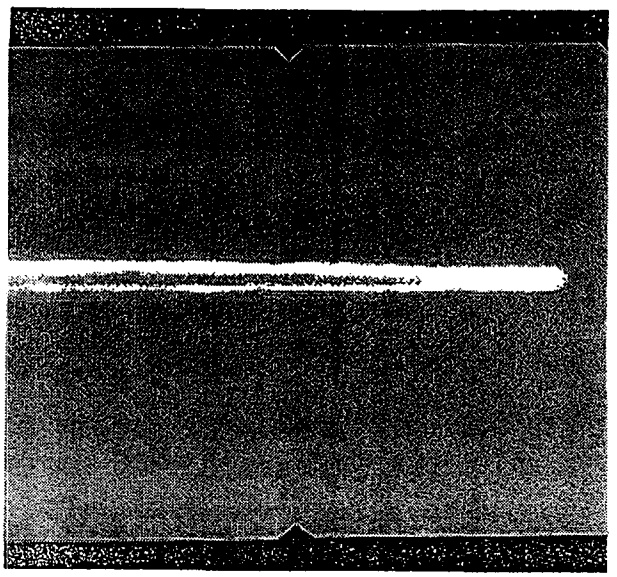

Figure 4. Super-fast 12.3 km/sec. Aluminum Jet from the 100 mm LX-14 Charge.

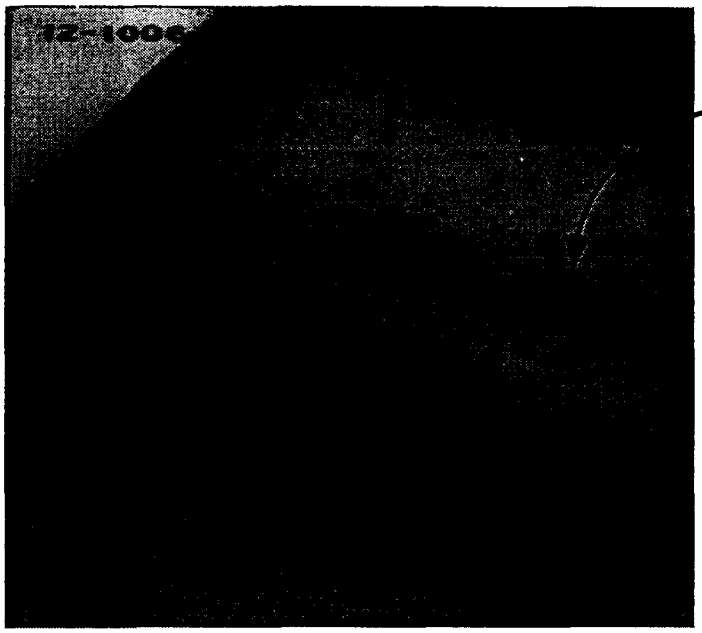

Figure 5.
Jet approaching third target element

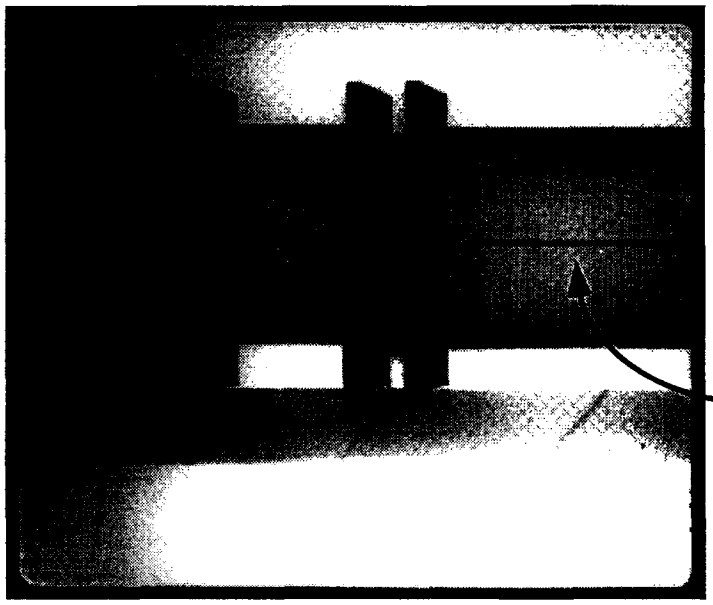

Figure 6.
Jet approaching third target component of simulated array

Figure 5. Jet from Aluminum-lined 100 mm LX-14 charge approaching the third target component in a spaced array: Appearance of the jet after penetrating through an oblique metal-explosive metal sandwich and a mild steel plate.

Figure 6. Appearance of the jet after penetrating an inert simulant of the explosive sandwich and a mild steel plate at normal incidence. Line of sight thickness for (5) and (6) were identical.

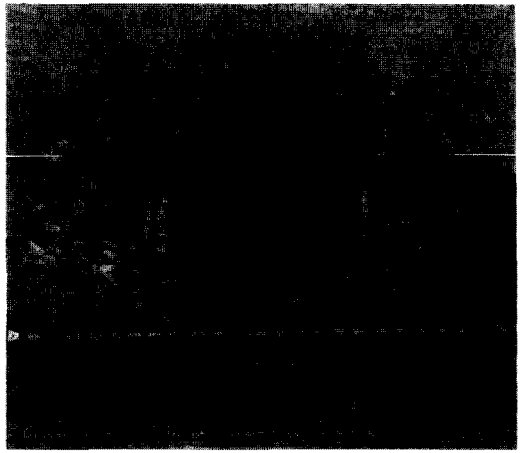

Figure 7. Through Hole Perforation Made by Super-Fast Jet from the 100 mm Aluminum Lined LX-14 Charge.

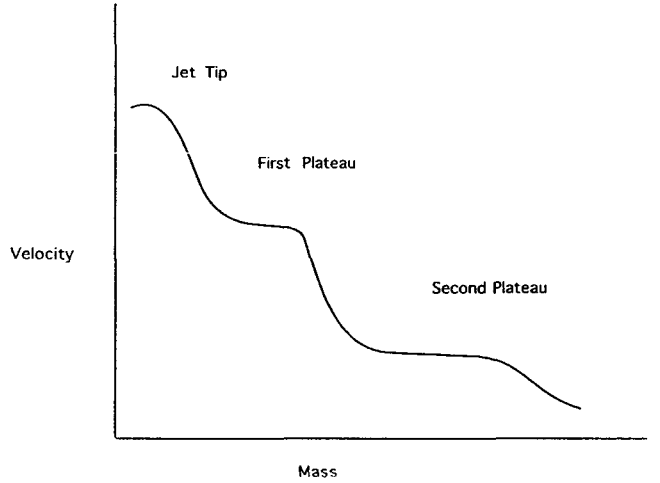

Figure 8. Velocity-Mass Distribution for Creative Localized Energy Packets In A Jet As Predicted by CTH. (For Comparison to Experimental Data See Figure 9).

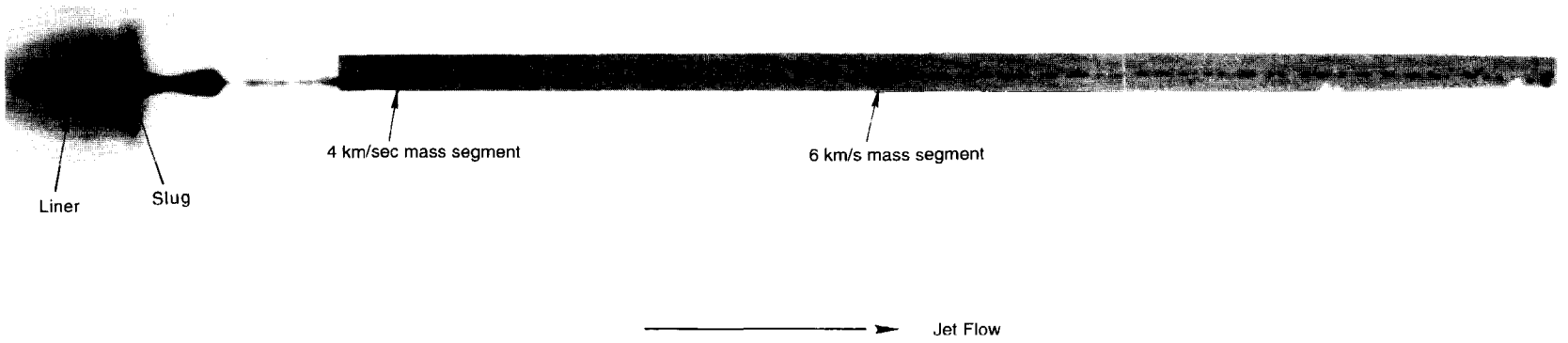

Figure 9. Jet With Designed Energetic Mass Segments.

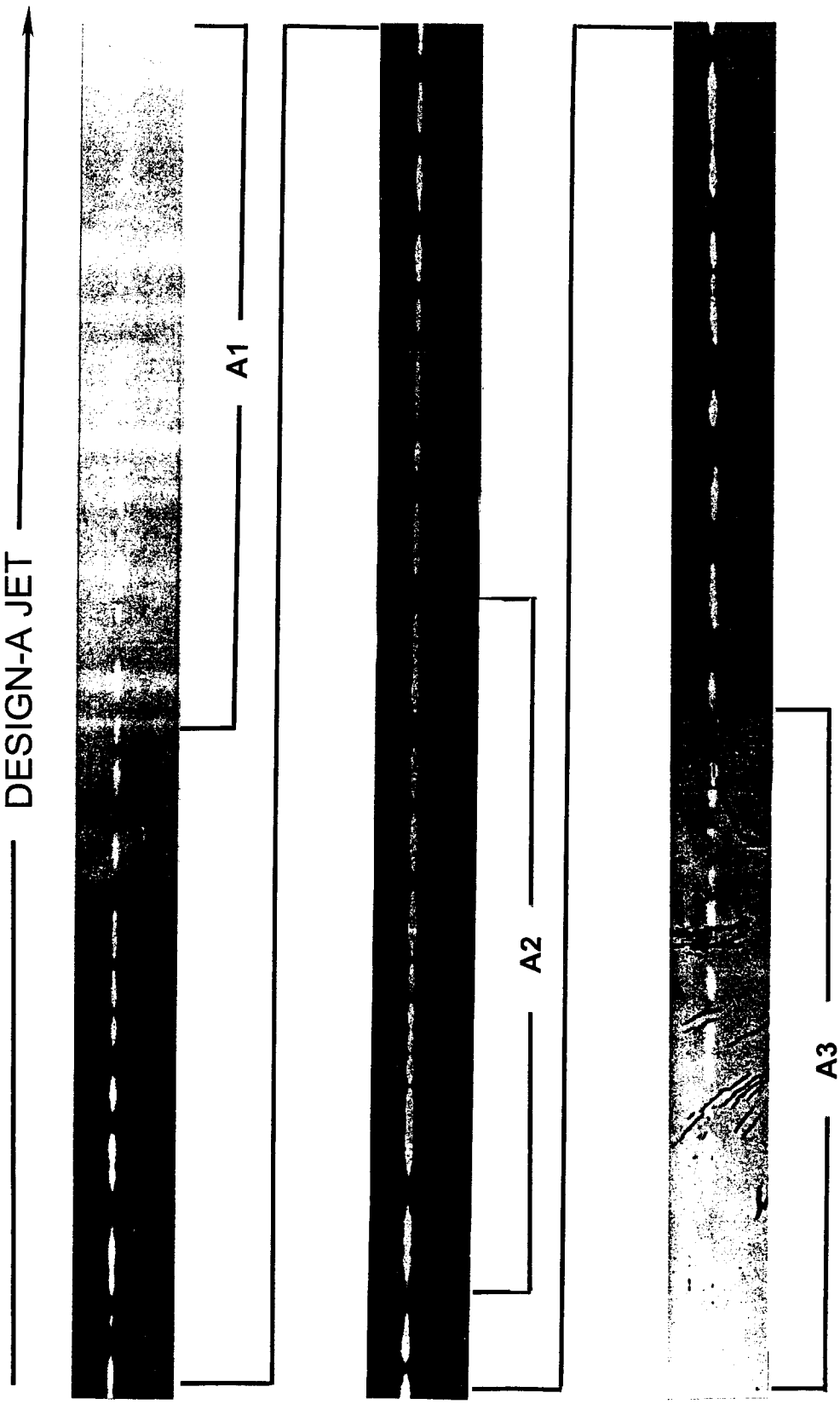

Figure 10. Design #1: Tip-To-Tail Composite Radiograph (Plate A1 Jet Tip, Plate A3 Jet Tail).

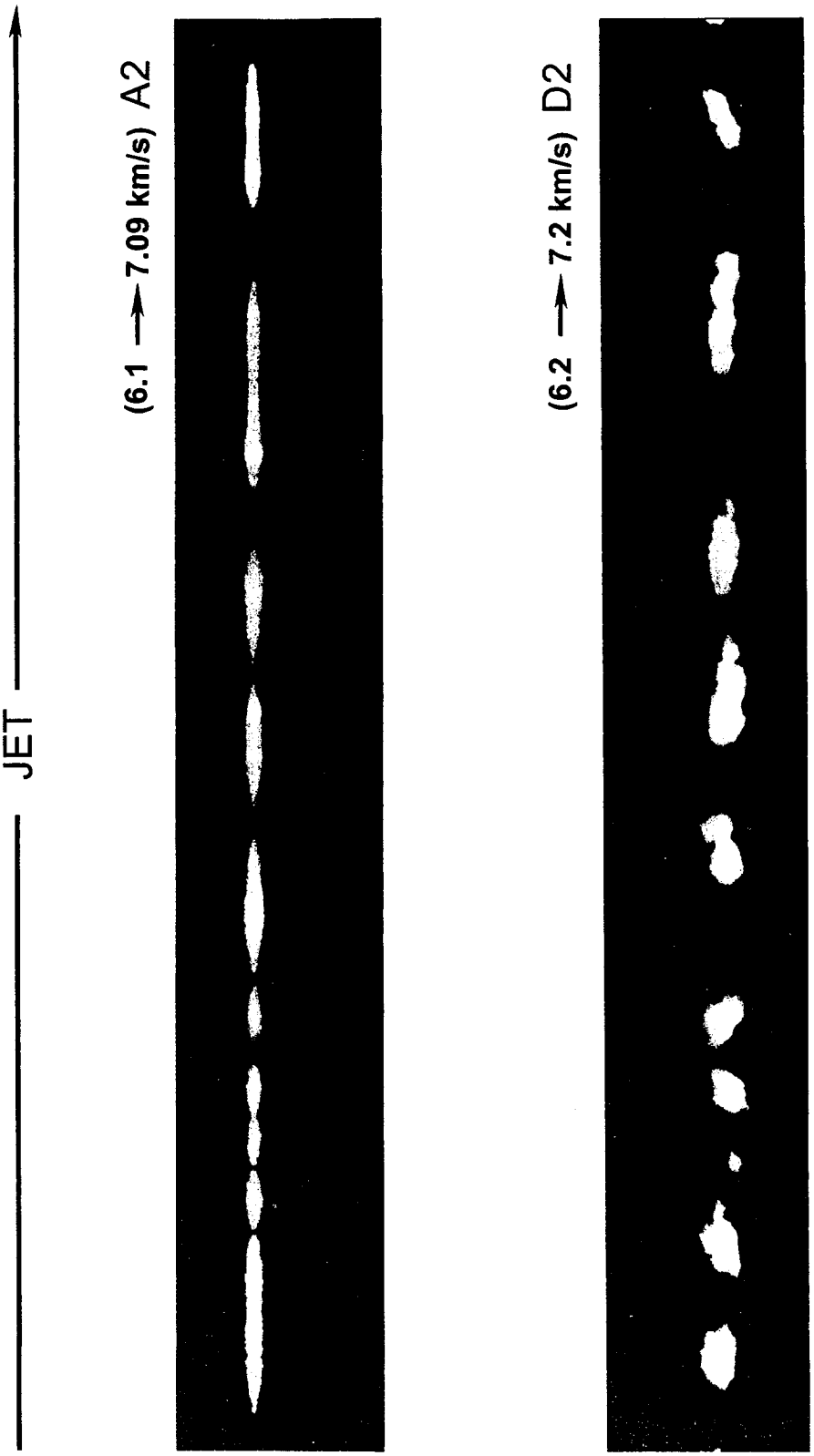

Figure 11. Radiographs Comparing Corresponding Mid-Length Sections of Design #1 (Plate A2) and Design #2 (Plate D2).

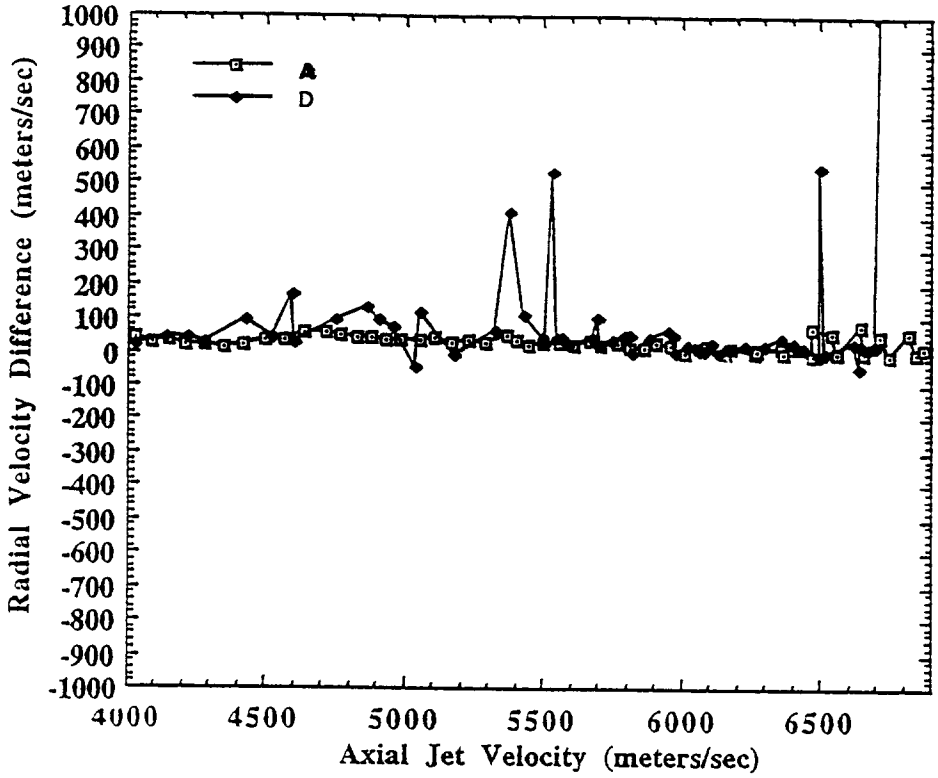

Figure 12. CTH Comparisons of Radial Velocity Gradients.